Absence of Cytotoxicity towards Microglia of Iron Oxide (α-Fe2O3) Nanorhombohedra

Journal:	*Toxicology Research*
Manuscript ID	TX-ART-11-2015-000421.R1
Article Type:	Paper
Date Submitted by the Author:	21-Jan-2016
Complete List of Authors:	Lewis, Crystal; Chemistry, Torres, Luisa; Stony Brook University, Miyauchi, Jeremy; Stony Brook University, Rastegar, Cyrus; Stony Brook University, Patete, Jon; Chemistry, Smith, Jacqueline; Stony Brook University, Wong, Stanislaus S; SUNY Stony Brook, Tsirka, Stella; Stony Brook University,

Absence of Cytotoxicity towards Microglia of Iron Oxide (α-Fe_2O_3) Nanorhombohedra

Crystal S. Lewis,[1,#], Luisa Torres [2,#] Jeremy T. Miyauchi[2#], Cyrus Rastegar,[2] Jonathan M. Patete,[1] Jacqueline M. Smith,[1] Stanislaus S. Wong,[1,3,*] and Stella E. Tsirka[2,*]

[1] Department of Chemistry, State University of New York at Stony Brook, Stony Brook, New York 11794-3400, USA

[2] Department of Pharmacological Sciences, State University of New York at Stony Brook, Stony Brook, New York 11794-8651, USA

[3]Condensed Matter Physics and Materials Science Department, Building 480, Brookhaven National Laboratory, Upton, New York 11973, USA

[#]These authors contributed equally to the work.

[*]Email: styliani-anna.tsirka@stonybrook.edu; stanislaus.wong@stonybrook.edu

Abstract. Understanding the nature of interactions between nanomaterials, such as commercially ubiquitous hematite (α-Fe_2O_3) Nanorhombohedra (N-Rhomb) and biological systems is of critical importance for gaining insight into the practical applicability of nanomaterials. Microglia represent the first line of defense in the central nervous system (CNS) during severe injury or disease such as Parkinson's and Alzheimer's disease as illustrative examples. Hence, to analyze the potential cytotoxic effect of nanorhombohedra exposure in the presence of microglia, we have synthesized Rhodamine B (RhB) labeled-α-Fe_2O_3 N-Rhomb, with lengths of 47 ± 10 nm and widths of 35 ± 8 nm. Internalization of RhB labeled-α-Fe_2O_3 N-Rhomb by microglia in the mouse brain was observed, and a dose-dependent increase in the cellular iron content as probed by cellular fluorescence was detected in cultured microglia after nanoparticle exposure. The cells maintained clear functional viability, exhibiting little to no cytotoxic effects after 24 and 48 hours at acceptable, physiological concentrations. Importantly, the nanoparticle exposure did not induce microglial cells to produce either tumor necrosis factor alpha (TNFα) or interleukin 1-beta (IL1β), two pro-inflammatory cytokines, nor did exposure induce the production of nitrites and reactive oxygen species (ROS), which are common indicators for the onset of inflammation. Finally, we propose that under the conditions of our experiments, i.e. in the presence of RhB labeled-α-Fe_2O_3 N-Rhomb maintaining concentrations of up to 100 μg/mL after 48 hours of incubation, the *in vitro* and *in vivo* internalization of RhB labeled-α-Fe_2O_3 N-Rhomb are likely to be clathrin-dependent, which represents a conventional mechanistic uptake route for most cells. Given the crucial role that microglia play in many neurological disorders, understanding the potential cytotoxic effects of these nanostructures is of fundamental importance if they are to be used in a therapeutic setting.

Keywords: α-Fe_2O_3 nanostructures, Microglia, Cytotoxicity, Neurotoxicity

1. Introduction

Nanomaterials, comprising nanoscale structures measuring between 1 and 100 nm in size, have attracted significant research interest due to their unique structure-dependent physical properties. Recently, concerns have been raised over the potentially deleterious effects of these nanomaterials on human health and the environment.[1-3] From a toxicological perspective, nanoscale materials can induce different types of cellular responses, characterized by a variety of distinctive uptake mechanisms, such as endocytosis, mediated for example by receptor-specific target sites.[4-6]

For a given nanomaterial, morphology (e.g. in terms of its size and shape) is thought to be one of the key factors that can decisively determine the observed degree of its cytotoxicity and cellular uptake. Indeed, significant effort, including from one of our groups in particular, has been involved with systematically synthesizing novel motifs of diverse classes of nanomaterials, such as but not limited to derivatized carbon nanotubes (CNTs), rare earth ion-doped cerium phosphate ($CePO_4$) nanowires, silicon dioxide (SiO_2) nanotubes, titanium dioxide (TiO_2) nanostructures, and zinc oxide (ZnO) nanowires and nanoparticles, to analyze their potential for biomedical applications. The objective of that prior body of work had been to correlate size, shape, morphology, and chemical composition of nanomaterials with their corresponding uptake mechanisms in an effort to probe and understand their individual and collective impact upon cellular toxicity, in general.[7-14] In effect, we had been interested in determining the specific factors that control nanoscale toxicity.

The model system we study herein is related to a family of magnetic iron oxide (Fe_3O_4) nanostructures that has already been well studied. Indeed, nanoparticulate magnetite have previously been extensively investigated for incorporation into diverse applications, including

for biological fluids, tissue-specific release of therapeutic agents, anti-cancer drug delivery systems, hyperthermia, and contrast enhancement for magnetic resonance imaging (MRI).[15-18] In this context, the study of their potential toxicology to cells has served as a valuable means of gauging the viability, biocompatibility, and overall practicality of this magnetic iron oxide platform for ubiquitous use in these assorted contexts.[19] Nevertheless, the use of Fe_3O_4 for biomedical applications has been limited by issues associated not only with particle inhomogeneity and cost concerns but also with its inability to effectively differentiate between tumors and artifacts arising from bleeding, metal deposits, and/or calcification in T_2-weighted MRI images.[20]

A common, companion material to Fe_3O_4, i.e. hematite (Fe_2O_3), possesses a rhombohedral crystal structure with a *R3c* space group.[21] However, unlike Fe_3O_4, hematite can exist in different crystallographic forms such as alpha-hematite (α-Fe_2O_3), beta-hematite (β-Fe_2O_3), gamma-hematite (γ-Fe_2O_3), and epsilon-hematite (ε-Fe_2O_3), with α-Fe_2O_3 and γ-Fe_2O_3 as the most familiar motifs. In particular, α-Fe_2O_3 has been synthesized as different morphologies, including as particles, cubes, and rods, and has been incorporated as functional components of gas sensors, CO oxidation catalysts, lithium-ion batteries, and colloidal mediators for hyperthermia treatment.[22-26] In a number of these aforementioned applications,[27] the α-Fe_2O_3 nanoparticles have been employed as particulate, aerosolized motifs. Therefore, it is imperative to understand the potential toxicological effect of exposure to nanoscale hematite, as manifested by different intake routes such as inhalation, ingestion, and injection.

Nevertheless, the intrinsic toxicity of Fe_2O_3 nanostructures still remains a matter of considerable controversy. For example, *in vitro* studies have shown that α-Fe_2O_3 nanoparticles larger than 90 nm in diameter (i.e. ~250 nm and ~1.2 μm) gave rise to little if any toxicity with

respect to human lung epithelial cells (A549) and murine alveolar macrophages (MH-S).[28] Moreover, α-Fe_2O_3 nanotubes, characterized by ~200 nm diameters, were found to be compatible with rat adrenal medulla cells (PC12), and in fact served as a potential delivery vehicle for nerve growth factor (NGF) in order to convert these cells into neurons.[29] By contrast, animal studies using Fe_2O_3 nanoparticles have revealed that these nanostructures may detrimentally induce either airway inflammation in healthy mice or cellular reduction in alveolus and lymph nodes in allergic mice.[30]

According to Brunauer-Emmett-Teller (BET) analysis, nanoscale rhombohedra, normalized for geometric considerations, possess a higher surface area (~45 m^2/g) than either nanocubes (~13.5 m^2/g) or nanorods (~39 m^2/g), depending on their size.[22, 31] Therefore, since the surface area of α-Fe_2O_3 N-Rhomb is second only to that of spherical nanoparticles (~133 m^2/g), which have already been extensively explored in cytotoxic analysis, this observation provides us with a rationale to fully understand the shape dependence of α-Fe_2O_3 N-Rhomb's interaction with cells, especially when engulfed.[32] Moreover, with various reports on the shape-dependent cytotoxic behavior of nanowires versus nanoparticles under various cellular conditions,[33] it is therefore necessary to gain a similar insight into the analogous effects of rhombohedral α-Fe_2O_3 in a biological context. In terms of a prior report with comparable objectives to our own, it is worth noting that studies involving $LiNbO_3$ nanorhombohedra have suggested that these nanostructures maintained cell viabilities of ~80% after 48 hours of incubation within mouse macrophage cells.[34]

Prior size and morphology-specific studies of various nanoparticles have indicated the ability of these nanoscale sized motifs to cross the blood brain barrier and thereby enter the central nervous system (CNS) of higher order biological organisms, such as mammals.[35, 36] In

light of this result, many metal oxides such as Fe_2O_3 and TiO_2 have been previously probed for possible neurotoxic effects upon exposure.[37-39] With α-Fe_2O_3 N-Rhomb's small size (<100 nm), large surface area, and chemical stability, nanoscale hematite possesses significant potential to overcome the challenges associated with passage through the blood brain barrier. Therefore, it represents an excellent system with which to probe cytotoxic effects associated with exposure of the CNS to nanomaterials, particularly nanostructures that have been surface modified through the attachment of different specific and judiciously chosen moieties.[40]

In this work, herein, we have synthesized visually traceable, dye-conjugated nanostructures, i.e. Rhodamine B (RhB)-labeled α-Fe_2O_3 N-Rhomb. Subsequently, we tested their uptake and possible toxicity in a key model system, i.e. microglia, the immuno-competent cells associated with the CNS. These cells are implicated in the pathology of many CNS disorders, including Alzheimer's disease, spinal cord injury, multiple sclerosis, Parkinson's disease, and ischemia.[41-47] Hence, given the central function and critical biological importance of microglia, our objective herein has been to understand the implication of their exposure to our iron oxide rhombohedral nanoparticles in order to determine any potential cytotoxic effects. To the best of our knowledge, our use of iron oxide nanorhombohedra to assess the distinctive role of the rhombohedral shape (and associated surface area) in the context of cytotoxicity has not been previously demonstrated in the literature. Herein, we reveal that microglia successfully incorporate RhB-labeled α-Fe_2O_3 N-Rhomb under both *in vivo* and *in vitro* conditions. More importantly, we definitively demonstrate that incubation with these nanoscale metal oxides at physiological concentrations in fact do not induce either cellular toxicity or inflammatory reactions in cultured microglia.

2. Experimental procedures

X-ray Diffraction

The crystallographic purity of as-prepared α-Fe_2O_3 N-Rhomb was confirmed using powder XRD. To prepare a typical sample for analysis, a fixed quantity was dispersed in ethanol and sonicated for ~1 min, prior to deposition onto a glass slide. Diffraction patterns were subsequently obtained using a Scintag diffractometer, operating in the Bragg configuration using Cu Kα radiation (λ = 1.54 Å) and with 2θ lattice parameters, ranging from 20 to 70° at a scanning rate of 0.25°/min for variously sized α-Fe_2O_3 N-Rhomb.

Primary microglial cultures and the N9 microglial cell line

Cerebral cortices from postnatal day 1 MacGreen mice, which express enhanced green fluorescent protein (eGFP) under the control of the microglia/macrophage-specific promoter CSF1R in the C57BL6 background,[48] were dissected, digested with trypsin (0.25% in HBSS) for 15 minutes at 37°C, and mechanically dissociated by trituration, as described previously.[49] Mixed cortical cells were plated in DMEM medium, consisting of 10% FBS, 1% sodium pyruvate, and gentamycin on poly-D-lysine coated tissue culture plates. After 10 days, microglial cells were separated from the astrocytic monolayer by the addition of 12 mM lidocaine, and the isolated microglia were seeded onto 24 well plates at a density of 15,000 cells/mL. The N9 immortalized murine microglial cell line was maintained under identical culture conditions.[50]

α-Fe_2O_3 N-Rhomb preparation for Cell Culture

Due to the direct mutual attraction between nanostructures *via* either van der Waals forces or chemical bonding, some degree of aggregation is expected.[51, 52] As a result, the α-Fe_2O_3 N-Rhomb stock solution (1 mg/mL), which was prepared using cell culture medium containing fetal bovine serum, was sonicated for 24 hours using a sonicator probe (220 - 260 V, 7.5 A,

Misonix Model XL2020) in order to break up the bulkier agglomerates of nanocrystals.

Quantification of Cell Fluorescence

MacGreen microglia were plated onto 24-well plates containing coverslips at a density of 15,000 cells/mL. Approximately 24 hours after plating, microglia were treated with 1 μg/mL, 10 μg/mL, and 100 μg/mL solutions of either bare RhB or RhB-labeled α-Fe_2O_3 N-Rhomb. After 24 hours, coverslips were fixed in 4% Paraformaldehyde (PFA) and mounted onto slides using 4',6-diamidino-2-phenylindole (DAPI) fluoromount. Five Z-Stack images were taken per cover slip at 63X magnification at a digital resolution of 1024 x 1024 with a Zeiss confocal microscope using LSM 510 Meta software. The fluorescence of each cell per image was quantified using ImageJ software. The corrected total cell fluorescence (CTCF) was calculated with the formula: CTCF = integrated density of cell – area of cell X mean gray area of a background sample. For experiments in which the mechanism of nanoparticle uptake was studied, MacGreen microglia were pre-treated with Chlorpromazine (CPZ) (Sigma- Aldrich) at a final concentration of 30 μM, approximately two hours before RhB-labeled α-Fe_2O_3 N-Rhomb exposure.

Electron microscopy

The morphology and size of the bare α-Fe_2O_3 nanostructures were assessed using a field emission SEM (FE-SEM Leo 1550) and an analytical high-resolution SEM (JEOL 7600F) instrument operating at an accelerating voltage of 15 kV, both of which were equipped with EDX capabilities. To prepare these samples for structural characterization, fixed amounts were dispersed in water and sonicated for ~1 min, prior to deposition onto a silicon (Si) wafer.

Low magnification transmission electron microscopy (TEM) was also used at an accelerating voltage of 120 kV using a JEOL JEM-1400 instrument, equipped with a 2048 x 2048 Gatan CCD digital camera as well as with energy dispersive X-ray (EDX) spectroscopy

capabilities. High-resolution TEM (HR-TEM) images coupled with SAED patterns were recorded using a JEOL JEM-3000F microscope, equipped with a Gatan image filter (GIF) spectrometer operating at an accelerating voltage of 300 kV. All samples were then primed for analysis by dispersion in water followed by sonication. Subsequently, the solution was deposited drop-wise onto a 300 mesh Cu grid.

To prepare the corresponding microglia engulfed RhB-labeled α-Fe_2O_3 nanostructures for TEM observation, microglia were plated onto ACLAR sheets (EMS, Hatfield, PA.) and treated with 1 μg/mL, 10 μg/mL, and 100 μg/mL of bare α-Fe_2O_3 N-Rhomb, respectively. Samples were then consigned to 2% osmium tetroxide in 0.1 M PBS, pH 7.4, dehydrated in a graded series of ethyl alcohol, and embedded with Durcupan resin. Samples were then placed onto formvar-coated slot copper grids, counter-stained with uranyl acetate and lead citrate, and later viewed with a FEI Tecnai12 BioTwinG^2 electron microscope. Digital images were acquired with an AMT XR-60 CCD Digital Camera system.

Enzyme Linked Immuno-Absorbent Assay (ELISA)

Conditioned medium, obtained from primary cell cultures respectively treated with 1 μg/mL, 10 μg/mL, and 100 μg/mL of α-Fe_2O_3 N-Rhomb, was used for ELISA analysis. Levels of tumor necrosis factor alpha (TNFα) and interleukin 1-beta (IL1β) were determined using the eBiosciences quantitative sandwich enzyme immunoassay following the manufacturer's protocol. Briefly, 96 well plates were coated with diluted Capture antibody and incubated overnight at 4°C. The plates were blocked for one hour at room temperature followed by a two-hour incubation period with either the standard or the sample. The wells were then incubated for 1 hr with a working detector solution followed by incubation with the substrate solution for 30 min. The reaction was stopped with 50 μL of 1N H_2SO_4. The absorbance of each well was

recorded using 450 nm wavelength light on an ELISA plate reader.

Lactate dehydrogenase (LDH) Cytotoxicity

An LDH Cytotoxicity Detection Kit (Roche Diagnostics Ltd) was used, according to the manufacturer's instructions. Briefly, primary microglia were incubated for 24 or 48 hours with different concentrations of α-Fe_2O_3 N-Rhomb. Samples were run in triplicate to determine LDH release by microglia in the presence of α-Fe_2O_3 N-Rhomb. Untreated cells served as a 'low control', whereas detergent-lysed cells served as a 'high control' for LDH release. 100 μL of the kit 'reaction mixture' was added to the wells. The plate was then maintained in the dark for 30 minutes at room temperature, to allow for the tetrazolium salt, INT, in the presence of LDH, to become reduced to formazan. The reactions were terminated by addition of 'stop' solution. Absorbance values of the formazan dye were measured at 490 nm using an ELISA plate reader. Cytotoxicity was calculated using the following equation: Cytotoxicity (%) = (experimental reading - low control reading) / (high control reading - low control reading) x 100%.

Nitric Oxide Assay

Nitric oxide (NO) production by microglia cultured in the presence of N-Rhomb was determined by the reaction of nitrite present in cell supernatant with 2, 3-diaminonaphthalene (DAN). Briefly, primary microglia were seeded in 96 well plates and exposed to the α-Fe_2O_3 N-Rhomb motifs for 24 h. The cultured supernatant was then collected and centrifuged to remove the N-Rhomb. 100 μL of cell supernatant and 20 μL DAN (0.05 mg/ml in 0.62 M HCl) were re-suspended together. The reaction was terminated after 20 minutes with the addition of 100 μL of 0.28 M NaOH. A Mithras LB 940 Multimode Microplate Reader (Berthold Technologies) was then used to measure 2,3-naphthyltriazole formation, using a 355 nm excitation / 460 nm emission filter pair. The nitrite concentrations in samples were calculated, based upon a sodium

nitrite standardization curve.

DCFDA Assay for the Detection of ROS

The production of reactive oxygen species (ROS) by microglia was measured using a 2', 7'-dichlorofluorescein diacetate (DCFDA) assay, as previously described.[53] Non-fluorescent DCFDA is converted to 2', 7'-dichlorofluorescein (DCF) in the presence of ROS. Briefly, microglia were plated onto a 96 well plate and incubated for 24 hours with different concentrations of N-Rhomb. After 24 hours, the media from the plates were aspirated off, and the cells were washed with 1x PBS followed by incubation with 25 μM DCFDA dissolved in 1x PBS for 30 minutes. The cells were then washed in 1x PBS, and the amount of DCF present within the cells was quantified on a Fluoroskan Ascent Microplate Fluorometer (Thermo Scientific) using a 485 nm excitation / 530 nm emission filter pair. The fluorescence of treated samples was standardized relative to untreated (i.e. negative) control cells. Cells incubated for 24 hours with 100 ng/mL lipopolysaccharide (LPS) served as a positive control for the production of ROS and the subsequent oxidation of DCFDA to DCF.

Animals

All experiments conducted had prior approval from the Institutional Animal Care and Use Committee (IACUC) as well as the Department of Laboratory Animal Research at Stony Brook University.

Intrahippocampal RhB- labeled α-Fe_2O_3 N-Rhomb injection

Injections were performed bilaterally in the hippocampus. Mice were anesthetized with 1.25% Avertin and injected with 100 μg/mL of RhB-labeled α-Fe_2O_3 N-Rhomb at stereotactic coordinates -2.5 mm from Bregma and -1.7 mm lateral using a Hamilton syringe (0.485 mm I.D., Hamilton, Reno, NV) connected to a motorized stereotaxic injector (Stoelting, Wood Dale, IL).

Following surgery, animals were injected intraperitoneally (i.p.) with 0.03 mg/kg of buprenorphine (Bedford labs) and left on a heating pad, until they were fully recovered from anesthesia. After 24 hours post-injection, mice were anesthetized and perfused with 4% PFA. The brains were collected, post-fixed, cryo-protected, and cut into 40 μm thick sections. The sections were then mounted with DAPI fluoromount, and photographed at a digital resolution of 1024 x 1024 with a Zeiss confocal microscope using LSM 510 Meta software.

Statistics

All statistics were performed using either Statview (v. 4.0) or GraphPad Prism 6 for Windows. Data are presented as mean ± SEM (i.e. standard error on the mean). One-way ANOVA was used to determine the level of significance between groups in the fluorescence quantification analysis, LDH test, and TNFα ELISA, respectively. A Bonferroni post-test was used to control for multiple comparisons. Data were considered to be statistically significant, when $p < 0.05$.

3. Results

Product Characterization of bare α-Fe_2O_3 N-Rhomb

We discuss the preparative protocols of our α-Fe_2O_3 N-Rhomb nanostructures in significant detail in the Supporting Information section. Specifically, using the hydrothermal technique at 120°C for 12 hours, we were able to generate both average-sized and small-sized α-Fe_2O_3 N-Rhomb, as determined by XRD (Figure 1C & D), with all of the expected diffraction peaks observed, corresponding to the standard JCPDS pattern for phase-pure hematite α-Fe_2O_3 (JCPDS #86-0550). Typical images associated with the SEM analysis of the smaller-sized and average-sized N-Rhomb, as shown in Figure 1, revealed that the nanostructures possessed the

correct morphology and were uniform in size, with associated measured lengths of 47 ± 10 nm and 75 ± 8 nm, and corresponding widths of 35 ± 8 nm and 50 ± 8 nm, respectively.

Cultured Microglia Engulf bare α-Fe_2O_3 N-Rhomb

When the CNS undergoes either injury, infection, or disease, microglia, i.e. the immuno-competent cells of the CNS, act as the first line of defense. They migrate to the site of injury, assume antigen-presenting properties, secrete cytokines, and trigger phagocytosis of dead cells and cell debris.[54]

To test the ability of microglia to internalize nano-sized α-Fe_2O_3 particles, N9 immortalized microglia were exposed to increasing concentrations of the smaller sized bare α-Fe_2O_3 N-Rhomb (Figure 2A). The cells were imaged with a light microscope, approximately 24 hours after exposure (Figure 2A). The light microscopy images shows that N9 microglia did indeed internalize α-Fe_2O_3 N-Rhomb and consequentially, remained viable after treatment, as the structural integrity of the membranes of the microglia cells had been maintained, even upon nanostructure incorporation (Figure 2A).

Electron microscopy images of primary C57BL6 microglia were also consistent with this observation. For each nanoparticulate concentration tested, these microglia cells were found to have incorporated ~47 nm α-Fe_2O_3 N-Rhomb primarily within the cellular vesicles as opposed to the nucleus (Figure 2B). In general, we found that the higher the initial incubation concentration, the greater the number of N-Rhomb particles observed within the microglia. Moreover, there was no sign of cytotoxicity, as the cells retained their resting state and shape (i.e. long branches with small cellular bodies). It is noteworthy that the larger-sized ~75 nm N-Rhomb were detected and incorporated to a lesser extent within the microglia cells as compared with the correspondingly smaller ~47 nm N-Rhomb (Figure S1). As a result, additional experiments were performed on

the smaller-sized ~47 nm nanorhombohedra.

To further confirm the presence of α-Fe_2O_3 N-Rhomb within the microglia cells themselves, chemically-sensitive EDX spectroscopy data were taken on two representative regions of the microglia (Figure S2). In one area, the hematite N-Rhomb structures appear to be clearly engulfed within the microglia cells (Free Draw 1), whereas in another part of the sample, no hematite nanorhombohedra are apparently visible (Free Draw 2). Based upon the EDX spectrum, the signals associated with the N-Rhomb-containing area gave rise to significantly higher peak intensities for Fe, i.e. ~ 7x larger, than for the area without N-Rhomb present. Therefore, these data are consistent with the idea of the iron oxide nanostructures as being localized and engulfed within the microglia cells, as expected. Other peaks such as copper (Cu), lead (Pb), and osmium (Os) emanate from the TEM copper grid as well as from the cross-sectional staining agents of lead citrate and osmium tetroxide, respectively.

To visualize the *in vitro* engulfment of the α-Fe_2O_3 N-Rhomb by microglia from an optical perspective, α-Fe_2O_3 N-Rhomb were labeled with the fluorescent dye RhB (95%, Aldrich) for easy detection (Figure 3A). We describe the chemical modification protocol used to conjugate α-Fe_2O_3 N-Rhomb with RhB both in words as well as schematically (Figure S3) in the Supporting Information section. Spectroscopic confirmation of the successful attachment and binding of the dye onto the iron oxide surface was provided by UV-visible and infrared (IR) spectroscopy data. The expected absorption and bond signatures noted in these results are consistent with the generation of RhB-labeled α-Fe_2O_3 N-Rhomb. These data are provided in the Supplemental Information section (Figure S4). Additionally, the engulfment behavior of RhB labeled N-Rhomb by primary microglia was compared with that of a bare RhB control (Figure S5). Primary microglia were obtained from neonatal MacGreen mice, which express eGFP under

the control of the microglia/macrophage promoter CSF1R in the C57BL6 background.[48] MacGreen microglia were exposed to increasing concentrations of both RhB-labeled α-Fe_2O_3 N-Rhomb and bare RhB in separate runs for 24 hours. The cells were fixed, mounted on slides, and imaged using a confocal microscope. The fluorescence intensity, emanating from both the RhB-labeled α-Fe_2O_3 N-Rhomb and bare RhB contained within each cell, was quantified using ImageJ (Figure 3C & Figure S5).

Figure 3 is consistent with increasing fluorescence intensity with increasing concentrations of RhB-labeled α-Fe_2O_3 N-Rhomb analyzed. Cells treated with 100 μg/mL of RhB-labeled α-Fe_2O_3 N-Rhomb possessed significantly higher total cell fluorescence especially when compared with not only untreated cells but also cells treated with 1 μg/mL and 10 μg/mL of RhB-labeled α-Fe_2O_3 N-Rhomb, thereby indicating that microglia do successfully internalize these nanostructures (Figure 3).

By comparison, the control RhB samples also substantiated a trend of increasing fluorescent intensity with increasing concentration (Figure S5). However, changes in the microglial morphology from the original resting to a more activated, amoeboid form were evident, when imaging cells treated with sample controls at concentrations of 10 μg/mL and higher (Figure S5). However, this did not appear to be true in the presence of RhB-labeled Fe_2O_3 N-Rhomb, as these microglia cells all maintained their inactive, ramified morphology.

Microglia engulf Rh-B-labeled α-Fe_2O_3 N-Rhomb in a clathrin-dependent manner

To investigate the mechanism underlying the internalization of RhB functionalized α-Fe_2O_3 N-Rhomb, we tested the effect of chlorpromazine (CPZ), a specific clathrin-mediated endocytosis inhibitor, on the ability of microglia to internalize RhB-labeled α-Fe_2O_3 N-Rhomb (Figure 3B).[55] Cultured MacGreen microglia were pre-treated with a high concentration (30 μM)

of CPZ for 2 hours prior to RhB-labeled α-Fe_2O_3 N-Rhomb exposure, as previously described.[55] Approximately 24 hours later, the cells were fixed, mounted, and imaged under a confocal microscope. Microglia maintained their resting morphology after CPZ treatment, and in effect, we observed that the concentration of CPZ induced little if any apparent toxic effects (Figure 3B).

The localization of RhB labeled Fe_2O_3 N-Rhomb outside the cellular membrane of the microglia cells under confocal microscopy conditions suggested a lack of engulfment of the nanostructures (Figure 3B). Fluorescence quantification shows that treatment with 30 μM CPZ significantly prevented as much as 96% of the potential uptake of RhB-labeled α-Fe_2O_3 N-Rhomb at all of the concentrations of nanoparticles tested from 1 μg/mL to 100 μg/mL, thereby supporting the idea that microglia primarily internalize these particles through a clathrin-dependent mechanism (Figure 3C).

RhB-labeled α-Fe_2O_3 N-Rhomb are not toxic to Microglia at therapeutic concentrations

To test the potential cytotoxicity of the RhB functionalized α-Fe_2O_3 N-Rhomb on cultured microglia, a lactate dehydrogenase (LDH) assay was used. LDH is rapidly released when the membranes of cells rupture, and hence, the presence of LDH in the supernatant is indicative of cell death.[56] As such, primary microglia were treated with increasing concentrations of RhB-labeled α-Fe_2O_3 N-Rhomb (Figure 4A), and the media were collected 24 and 48 hours later so as to measure LDH release. As Figure 4A shows, both untreated and treated microglia exhibited similar levels of LDH release and displayed less than ~4% cytotoxicity at 24 hours. After 48 hours, a significant increase of ~30% cytotoxicity was observed in microglia treated with the highest concentration of NRhomb (i.e. 100 μg/mL). Nevertheless, it should be noted that this concentration is approximately 626 μM, which far exceeds a normal therapeutic dose. All of

the other concentrations tested exhibited no apparent cytotoxicity over the period of time tested.

RhB-labeled α-Fe_2O_3 N-Rhomb do not cause *in vitro* microglial activation

Microglia can give rise to at least two different activation states, depending on the signals they receive: the pro-inflammatory M1 state and the anti-inflammatory M2 state. In the M1 state, microglia secrete tumor necrosis factor alpha (TNFα), interleukin-1 beta (IL1β), and other pro-inflammatory cytokines, while in the M2 state, microglia produce IL-10, IL-4, TGF-β, as well as other anti-inflammatory factors. In several injury models, M2 microglia have been deemed to be beneficial for tissue regeneration,[57, 58] whereas M1 microglia are considered to inhibit tissue healing and repair. Upregulation of TNFα has been found in previous literature to be implicated as a factor in various ailments such as Alzheimer's disease, cancer, major depression, and inflammatory bowel disease.[59-63]

To evaluate whether RhB-labeled α-Fe_2O_3 N-Rhomb result in microglial release of pro-inflammatory factors, ELISAs were performed to quantify the levels of the pro-inflammatory cytokines TNFα and IL1β. Primary microglia were treated with increasing concentrations of RhB-labeled α-Fe_2O_3 N-Rhomb, and the media were collected approximately 24 hours later to measure corresponding levels of TNFα and IL1β (Figure 4B & C).

Exposure to lipopolysaccharide (LPS) was used as a positive control since it is a potent inducer of pro-inflammatory cytokines in microglia.[64] After 24 hours, there was no significant increase in the levels of either TNFα or IL1β produced by microglia that had been treated with systematically greater concentrations (i.e. 1, 10, or 100 μg/mL) of RhB-labeled α-Fe_2O_3 N-Rhomb, relative to the control. As expected, the levels of TNFα and IL1β released by LPS-treated cells were significantly higher than those produced by both untreated cells (i.e. control) as well as the cells treated with RhB-labeled α-Fe_2O_3 N-Rhomb, thereby confirming that the

presence of these nanoparticles does not necessarily give rise to the expression of pro-inflammatory agents.

RhB-labeled α-Fe_2O_3 N-Rhomb do not trigger either nitric oxide or ROS production *in vitro*

It is well known that nitric oxide (NO) is associated with various key functions within the CNS, such as regulation of synaptic plasticity, the sleep-wake cycle, and hormone secretion.[65, 66] However, when produced in excess, NO can undergo oxidation reduction reactions through the formation of reactive oxygen species (ROS), thereby generating reactive nitrogen-containing species that can result in nitrosative stress and cellular damage.[65, 66] Nitrite production by microglia after engulfment of N-Rhomb remained low, suggesting that the presence of varying concentrations of N-Rhomb did not result in the production of NO by microglia (Figure 4D). All concentrations of RhB-labeled N-Rhomb particles tested gave rise to insignificant changes in NO production by microglia, relative to untreated, control cells. Moreover, their NO production was significantly lower than that of a positive LPS control. Hence, it can be concluded that the presence of RhB labeled N-Rhomb alone does not induce noticeable NO production in microglia.

The production of ROS by microglia was also assessed using a DCFDA assay. DCFDA is esterified and oxidized by cells in the presence of ROS, giving rise to the fluorescent compound, DCF. Microglia treated with LPS served as a positive control for the production of ROS and, by extension, the intracellular accumulation of DCF. Cells treated with increasing concentrations of N-Rhomb showed no significant elevation in DCF accumulation relative to that of control samples, i.e. untreated cells, a finding indicative of negligible production of ROS (Figure 4E). Thus, it was determined that concentrations of NRhomb of up to 100 μg/mL did not induce ROS production in microglia *in vitro*.

Microglia internalize RhB-labeled α-Fe_2O_3 N-Rhomb *in vivo*

To test whether microglia can internalize RhB-labeled α-Fe_2O_3 N-Rhomb *in vivo*, MacGreen mice were injected with 100 μg/mL of RhB-labeled α-Fe_2O_3 N-Rhomb bilaterally into the dorsal hippocampus. Approximately 24 hours after the injection, the mice were transcardially perfused with 4% PFA; the brains were then collected, cryo-protected, sectioned into 40-μm thick slices, mounted, and imaged under a confocal microscope. White arrows in Figure 5 point towards microglia that have internalized RhB-labeled α-Fe_2O_3 N-Rhomb. Taken together, these data indicate that microglia can engulf α-Fe_2O_3 nanostructures under both *in vitro* and *in vivo* conditions in a clathrin-dependent manner without causing microglia to release pro-inflammatory factors which might have thereby compromised the viability of the cells.

4. Discussion

We have synthesized RhB labeled α-Fe_2O_3 N-Rhomb, and tested the ability of microglia to internalize them. These cells appear to efficiently engulf the RhB functionalized α-Fe_2O_3 N-Rhomb without any noticeable membrane damage, as suggested by electron and confocal microscopy. In terms of addressing potential shape-dependent toxicity, RhB-labeled α-Fe_2O_3 N-Rhomb are non-inflammatory and non-cytotoxic at therapeutic concentrations, suggesting that α-Fe_2O_3 N-Rhomb have the potential to be used as drug carriers. Drugs that either reduce M1 activation or induce M2 activation such as minocycline, tuftsin (TKPR), or microglia inhibitory factor (MIF/TKP)[67-69] could be conjugated onto nanoparticles in order to alter the phenotype of microglia. For instance, Papa et al. showed that nanostructures conjugated onto minocycline are engulfed by microglia and reduce inflammation in a model of spinal cord injury.[55]

Our results thus show promise for future studies involving the conjugation of anti-

inflammatory compounds onto nanostructures that can be engulfed by microglia as well as for the tracking of cell behavior using imaging techniques such as confocal microscopy and MRI, for example. This point has been demonstrated by some of our unpublished work (data not shown), in which we have observed that α-Fe_2O_3 N-Rhomb can be detected within a mouse brain by using T_2-weighted MRI scans.

We have been able to demonstrate that microglia can internalize both bare and RhB labeled N-Rhomb. Particle aggregation is expected due to the direct mutual attraction between nanostructures occurring via either van der Waals forces or chemical bonding.[51, 52] Sonication of the RhB labeled N-Rhomb prior to exposure to microglia reduced the degree of particle aggregation, although it did not completely prevent clustering. Due to the low TNFα, IL-1β, ROS, and nitrite levels in microglia after the RhB-labeled N-Rhomb treatment, it is unlikely that microglia themselves became over-activated, thereby resulting in an engulfment of a large amount of particles. The particle clusters observed in Figure 2 are more likely the result of aggregation, due to strong mutual attraction between these nanostructures.

Microglia are highly phagocytic and can clear away dead cells and debris using a variety of endocytic mechanisms, including receptor-mediated endocytosis, pinocytosis, and phagocytosis.[70-72] Indeed, microglia play key roles in several neurological diseases and can quickly respond to either infection or injury.[73, 74] Chemically modified nanostructures that can be easily engulfed by microglia represent therefore a potentially viable strategy with which to manipulate the functional properties of the microglia themselves.

Specifically, we have shown that microglia used a clathrin-dependent endocytic pathway to internalize RhB-labeled α-Fe_2O_3 N-Rhomb, as evidenced by the lack of nanoparticle uptake even at varying concentration levels, in the presence of the endocytosis inhibitor, CPZ. This

observation is in agreement with other studies that have successfully demonstrated internalization of other types of nanostructures by microglia.[55, 75, 76] Additionally, we have highlighted that internalization does not lead to aberrant activation in cultured microglia, i.e. in the presence of RhB labeled-α-Fe_2O_3 N-Rhomb maintaining concentrations of up to 100 μg/mL, and that microglia in the mouse brain are equally efficient at internalizing hematite nanostructures, thereby indicating that α-Fe_2O_3 N-Rhomb may be suitable for coupling anti-inflammatory agents as a form of drug therapy.

5. Acknowledgements:

Research (including support for LT and CSL) was provided by the Turner Dissertation fellowship (LT) and the Alliance for Graduate Education and Professoriate – Transformation (AGEP-T), which is funded by National Science Foundation - Division of Human Resources Development Contract No. HRD 1311318. Research funds were provided by the U.S. Department of Energy, Basic Energy Sciences, Materials Sciences and Engineering Division (JMP and SSW), NIH T32GM007518 (JTM), and NIH R01NS42168 (SET), respectively. Experiments were performed in part at the Center for Functional Nanomaterials located at Brookhaven National Laboratory, which is supported by the U.S. Department of Energy under contract number DE-SC-00112704. Transmission electron microscopy data acquired for our microglia experiments were collected at the Center Microscopy Imaging Center (C-MIC) at Stony Brook University, Stony Brook, NY 11794 under the direction of Ms. Susan Van Horn.

References

1. V. Colvin, *Nat. Biotech.*, 2003, **21**, 1166-1170.
2. C. S. S. R. Kumar, ed., *Nanomaterials: toxicity, health and environmental issues*, Wiley-VCH, Weinheim, 2006.
3. N. Lewinski, V. Colvin and R. Drezek, *Small*, 2008, **4**, 26-49.
4. W. Li, C. Chen, C. Ye, T. Wei, Y. Zhao, F. Lao, Z. Chen, H. Meng, Y. Gao, H. Yuan, G. Xing, F. Zhao, Z. Chai, X. Zhang, F. Yang, D. Han, X. Tang and Y. Zhang, *Nanotechnology*, 2008, **19**, 145102.
5. J. Sudimack and R. J. Lee, *Advanced Drug Delivery Review*, 2000, **41**, 147-162.
6. W. H. Suh, K. S. Suslick, G. D. Stucky and Y.-H. Suh, *Progress in Neurobiology*, 2009, **87**, 133-170.
7. S. Chen, X. Zhao, J. Chen, J. Chen, S. S. Wong and I. Ojima, *Bioconjugate Chemistry*, 2010, **21**, 979-987.
8. F. Zhang and S. S. Wong, *American Chemistry Society Nano*, 2010, **4**, 99-112.
9. H. Zhou, J. Chen, E. Sutter, M. Feygenson, M. C. Aronson and S. S. Wong, *Small*, 2010, **6**, 412-420.
10. J. Chen, H. Zhou, A. C. Santulli and S. S. Wong, *Chemical Research in Toxicology*, 2010, **23**, 871-879.
11. B. J. Panessa-Warren, J. Warren, S. S. Wong and J. A. Misewich, *Journal of Physics: Condensed Matter*, 2006, **18**, S2185-S2201.
12. A. Magrez, L. Horváth, R. Smajda, V. Salicio, N. Pasquier, L. Forró and B. Schwaller, *ACS Nanoscience & Nanotechnology*, 2009, **3**, 2274-2280.
13. C. Jin, Y. Tang, F. Yang, X. Li, S. Xu, X. Fan, Y. Huang and Y. Yang, *Biological Trace Element Research*, 2011, **141**, 3-15.
14. G. Tejral, N. R. Panyala and J. Havel, *Journal of Applied Biomedicine*, 2009, **7**, 1-13.
15. Z. Q. Samra, S. Shabir, Z. Rehmat, M. Zaman, A. Nazir, N. Dar and M. A. Athar, *Applied Biochemistry and Biotechnology*, 2010, **162**, 671-686.
16. Y. Ling, K. Wei, Y. Luo, X. Gao and S. Zhong, *Biomaterials*, 2011, **32**, 7139-7150.
17. B. Polyak and G. Friedman, *Expert Opinion on Drug Delivery*, 2009, **6**, 53-70.
18. Y. Wang, *Quantitative Imaging in Medicine and Surgery*, 2011, **1**, 35-40.
19. S. Xu, F. Yang, X. Zhou, Y. Zhuang, B. Liu, Y. Mu, X. Wang, H. Shen, G. Zhi and D. Wu, *ACS Applied Materials & Interfaces*, 2015, **7**, 20460-20468.
20. M. Z. Iqbal, X. Ma, T. Chen, L. Zhang, W. Ren, L. Xiang and A. Wu, *Journal of Materials Chemistry B: Materials for Biology and Medicine*, 2015, **3**, 5172-5181.
21. M. Catti, G. Valerio and R. Dovesi, *Physical Review B: Condensed Matter*, 1995, **51**, 7441-7450.
22. H. Liang, X. Jiang, Z. Qi, W. Chen, Z. Wu, B. Xu, Z. Wang, J. Mi and Q. Li, *Nanoscale* 2014, **6**, 7199-7203.
23. G. Wang, W. Li, K. Jia, B. Spliethoff, F. Schüth and A. Lu, *Applied Catalysis A: General*, 2009, **364**, 42-47.
24. S. Xu, C. M. Hessel, H. Ren, R. Yu, Q. Jin, M. Yang, H. Zhao and D. Wang, *Energy & Environmental Science*, 2014, **7,** 632-637.
25. G. Tong, J. Guan and Q. Zhang, *Materials Chemistry and Physics*, 2011, **127**, 371-378.
26. P. Basnet, G. K. Larsen, R. P. Jadeja, Y.-C. Hung and Y. Zhao, *Applied Materials & Interfaces*, 2013, **5**, 2085-2095.

27. J. M. Berg, S. Ho, W. Hwang, R. Zebda, K. Cummins, M. P. Soriaga, R. Taylor, B. Guo and C. M. Sayes, *Chemical Research in Toxicology*, 2010, **23**, 1874-1882.
28. F. S. Freyria, B. Bonelli, M. Tomatis, M. Ghiazza, E. Gazzano, D. Ghigo, E. Garrone and B. Fubini, *Chemical Research in Toxicology*, 2012, **25**, 850-861.
29. L. Chen, J. Xie, J. Yancey, M. Srivatsan and V. K. Varadan, *Journal of Nanotechnology in Engineering and Medicine*, 2010, **1**, 041014/041011-041014/041015.
30. Å. Gustafsson, U. Bergström, L. Ågren, L. Österlund, T. Sandström and A. Buchta, *Toxicology and Applied Pharmacology*, 2015, **288**, 1-11.
31. Y. Zhao, F. Pan, H. Li, T. Niu, G. Xu and W. Chen, *Journal of Materials Chemistry A*, 2013, **1**, 7242-7246.
32. L. E. Barton, A. N. Quicksall and P. A. Maurice, *Geomicrobiology Journal*, 2012, **29**, 314-322.
33. A. Adili, S. Crowe, M. F. Beaux, T. Cantrell, P. J. Shapiro, D. N. McIlroy and K. E. Gustin, *Nanotoxicology*, 2008, **2**, 1-8.
34. Y. Wang, X. Y. Zhou, Z. Chen, B. Cai, Z. Z. Ye, C. Y. Gao and J. Y. Huang, *Appl Phys a-Mater*, 2014, **117**, 2121-2126.
35. P. R. Lockman, M. O. Oyewumi, J. M. Koziara, K. E. Roder, R. J. Mumper and D. D. Allen, *Journal of Controlled Release*, 2003, **93**, 271-282.
36. B. T. Farrell, B. E. Hamilton, E. Dósa, E. Rimely, M. Nasseri, S. Gahramanov, C. A. Lacy, E. P. Frenkel, N. D. Doolittle, P. M. Jacobs and E. A. Neuwelt, *Neurology*, 2013, **81**, 256-263.
37. Y. Wang, B. Wang, M. T. Zhu, M. Li, H. J. Wang, M. Wang, H. Ouyang, Z. F. Chai, W. Y. Feng and Y. L. Zhao, *Toxicol Lett*, 2011, **205**, 26-37.
38. B. Wang, W. Y. Feng, M. T. Zhu, Y. Wang, M. Wang, Y. Q. Gu, H. Ouyang, H. J. Wang, M. Li, Y. L. Zhao, Z. F. Chai and H. F. Wang, *J Nanopart Res*, 2009, **11**, 41-53.
39. J. X. Wang, C. Y. Chen, Y. Liu, F. Jiao, W. Li, F. Lao, Y. F. Li, B. Li, C. C. Ge, G. Q. Zhou, Y. X. Gao, Y. L. Zhao and Z. F. Chai, *Toxicol Lett*, 2008, **183**, 72-80.
40. M. Mahmoudi, S. Sant, B. Wang, S. Laurent and T. Sen, *Advanced Drug Delivery Reviews*, 2011, **63**, 24-46.
41. L. J. Chew, P. Fusar-Poli and T. Schmitz, *Dev Neurosci*, 2013, **35**, 102-129.
42. Y. Deng, J. Lu, V. Sivakumar, E. A. Ling and C. Kaur, *Brain Pathol*, 2008, **18**, 387-400.
43. J. E. Merrill and N. J. Scolding, *Neuropathol Appl Neurobiol*, 1999, **25**, 435-458.
44. L. Peferoen, M. Kipp, P. van der Valk, J. M. van Noort and S. Amor, *Immunology*, 2014, **141**, 302-313.
45. M. Domercq, A. Perez-Samartin, D. Aparicio, E. Alberdi, O. Pampliega and C. Matute, *Glia*, 2010, **58**, 730-740.
46. M. M. Varnum and T. Ikezu, *Arch Immunol Ther Exp (Warsz)*, 2012, **60**, 251-266.
47. Z. Gao and S. E. Tsirka, *Neurol Res Int*, 2011, **2011**, 383087.
48. R. T. Sasmono, A. Ehrnsperger, S. L. Cronau, T. Ravasi, R. Kandane, M. J. Hickey, A. D. Cook, S. R. Himes, J. A. Hamilton and D. A. Hume, *J Leukoc Biol*, 2007, **82**, 111-123.
49. R. Bronstein, L. Torres, J. C. Nissen and S. E. Tsirka, *J Vis Exp*, 2013, DOI: 10.3791/50647.
50. B. Stansley, J. Post and K. Hensley, *J Neuroinflamm*, 2012, **9**, 115.
51. R. J. Hunter, *Foundations of Colloid Science*, Oxford University Press, New York, 1987.
52. D. Li and R. B. Kaner, *Journal of the American Chemical Society*, 2006, **128**, 968-975.
53. A. D. Harrington, S. E. Tsirka and M. A. A. Schoonen, *Chemosphere*, 2013, **93**, 1216-

1221.
54. K. Nakajima and S. Kohsaka, *The Journal of Biochemistry*, 2001, **130**, 169-175.
55. S. Papa, F. Rossi, R. Ferrari, A. Mariani, M. De Paola, I. Caron, F. Fiordaliso, C. Bisighini, E. Sammali, C. Colombo, M. Gobbi, M. Canovi, J. Lucchetti, M. Peviani, M. Morbidelli, G. Forloni, G. Perale, D. Moscatelli and P. Veglianese, *ACS Nano*, 2013, **7**, 9881-9895.
56. F. K. Chan, K. Moriwaki and M. J. De Rosa, *Methods Mol Biol*, 2013, **979**, 65-70.
57. K. A. Kigerl, J. C. Gensel, D. P. Ankeny, J. K. Alexander, D. J. Donnelly and P. G. Popovich, *J Neurosci*, 2009, **29**, 13435-13444.
58. V. E. Miron, A. Boyd, J. W. Zhao, T. J. Yuen, J. M. Ruckh, J. L. Shadrach, P. van Wijngaarden, A. J. Wagers, A. Williams, R. J. Franklin and C. ffrench-Constant, *Nat Neurosci*, 2013, **16**, 1211-1218.
59. D. Brenner, H. Blaser and T. W. Mak, *Nat Rev Immunol*, 2015, **15**, 362-374.
60. R. M. Locksley, N. Killeen and M. J. Lenardo, *Cell*, 2001, **104**, 487-501.
61. W. Swardfager, K. Lanctot, L. Rothenburg, A. Wong, J. Cappell and N. Herrmann, *Biol Psychiatry*, 2010, **68**, 930-941.
62. Y. Dowlati, N. Herrmann, W. Swardfager, H. Liu, L. Sham, E. K. Reim and K. L. Lanctot, *Biol Psychiatry*, 2010, **67**, 446-457.
63. J. Brynskov, P. Foegh, G. Pedersen, C. Ellervik, T. Kirkegaard, A. Bingham and T. Saermark, *Gut*, 2002, **51**, 37-43.
64. Y. Nakamura, Q. S. Si and K. Kataoka, *Neurosci Res*, 1999, **35**, 95-100.
65. P. Pacher, J. S. Beckman and L. Liaudet, *Physiological Reviews*, 2007, **87**, 315-424.
66. V. Calabrese, C. Mancuso, M. Calvani, E. Rizzarelli, D. A. Butterfield and A. M. Stella, *Nature Reviews Neuroscience*, 2007, **8**, 766-775.
67. J. C. Nissen, D. L. Selwood and S. E. Tsirka, *J Neurochem*, 2013, DOI: 10.1111/jnc.12404.
68. K. Kobayashi, S. Imagama, T. Ohgomori, K. Hirano, K. Uchimura, K. Sakamoto, A. Hirakawa, H. Takeuchi, A. Suzumura, N. Ishiguro and K. Kadomatsu, *Cell Death Dis*, 2013, **4**, e525.
69. J. Emmetsberger and S. E. Tsirka, *Neurobiol Dis*, 2012, **47**, 295-309.
70. N. B. Caberoy, G. Alvarado and W. Li, *J Neuroimmunol*, 2012, **252**, 40-48.
71. P. A. Ranson and W. E. Thomas, *J Histochem Cytochem*, 1991, **39**, 853-858.
72. S. Papa, R. Ferrari, M. De Paola, F. Rossi, A. Mariani, I. Caron, E. Sammali, M. Peviani, V. Dell'Oro, C. Colombo, M. Morbidelli, G. Forloni, G. Perale, D. Moscatelli and P. Veglianese, *J Control Release*, 2014, **174**, 15-26.
73. C. Colton and D. M. Wilcock, *CNS Neurol Disord Drug Targets*, 2010, **9**, 174-191.
74. A. D. Kraft and G. J. Harry, *Int J Environ Res Public Health*, 2011, **8**, 2980-3018.
75. M. R. Pickard and D. M. Chari, *Int J Mol Sci*, 2010, **11**, 967-981.
76. E. M. Luther, C. Petters, F. Bulcke, A. Kaltz, K. Thiel, U. Bickmeyer and R. Dringen, *Acta Biomater*, 2013, **9**, 8454-8465.

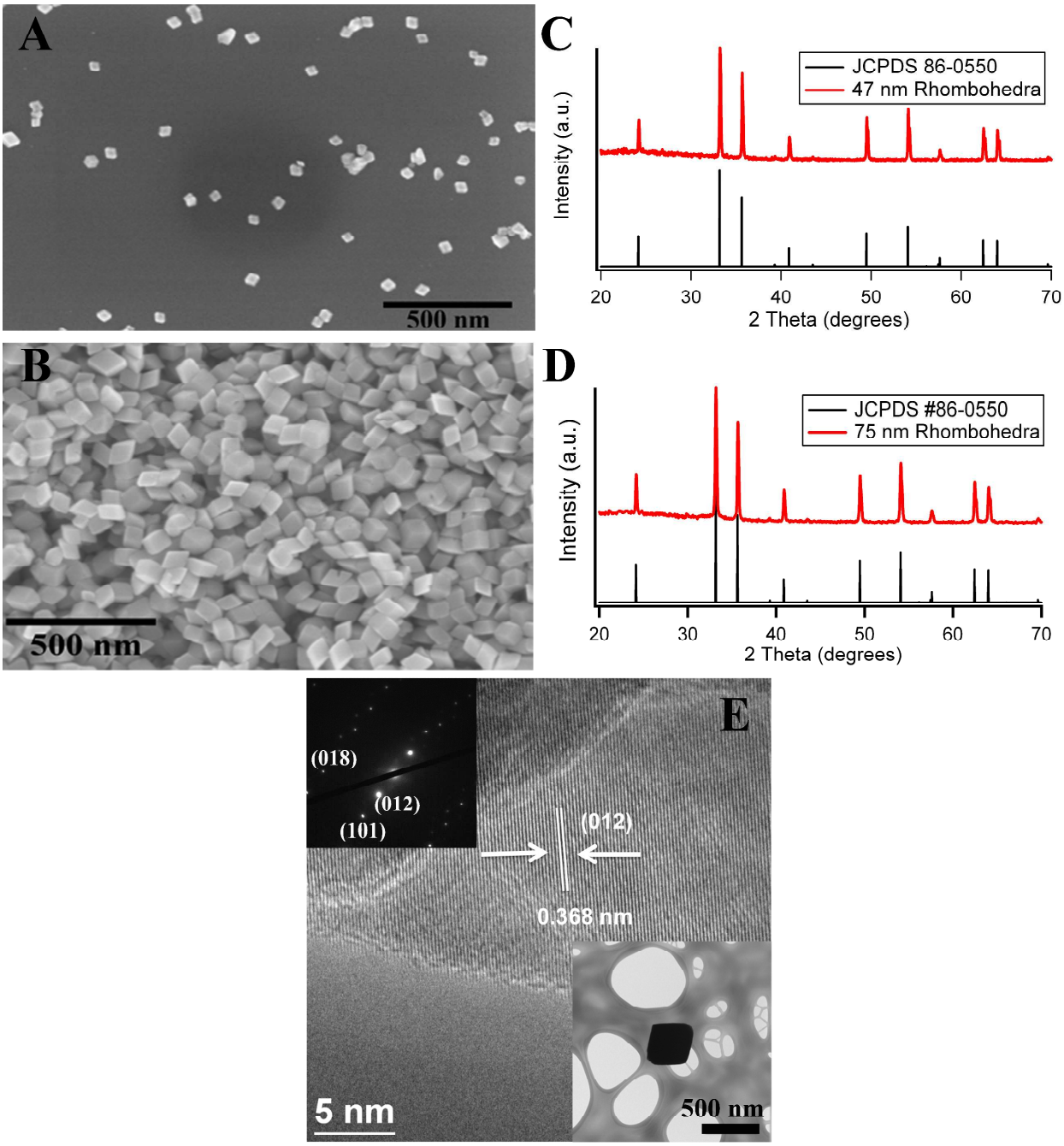

Figure 1. Characterization of small and average sized bare α-Fe_2O_3 N-Rhomb. (**A&C**) SEM and XRD images of small and average-sized (**B & D**) α-Fe_2O_3 N-Rhomb. (**E**). High-resolution TEM image of bare α-Fe_2O_3 N-Rhomb. A low magnification image in the lower right-hand inset is shown. The upper left-hand inset shows the electron diffraction pattern.

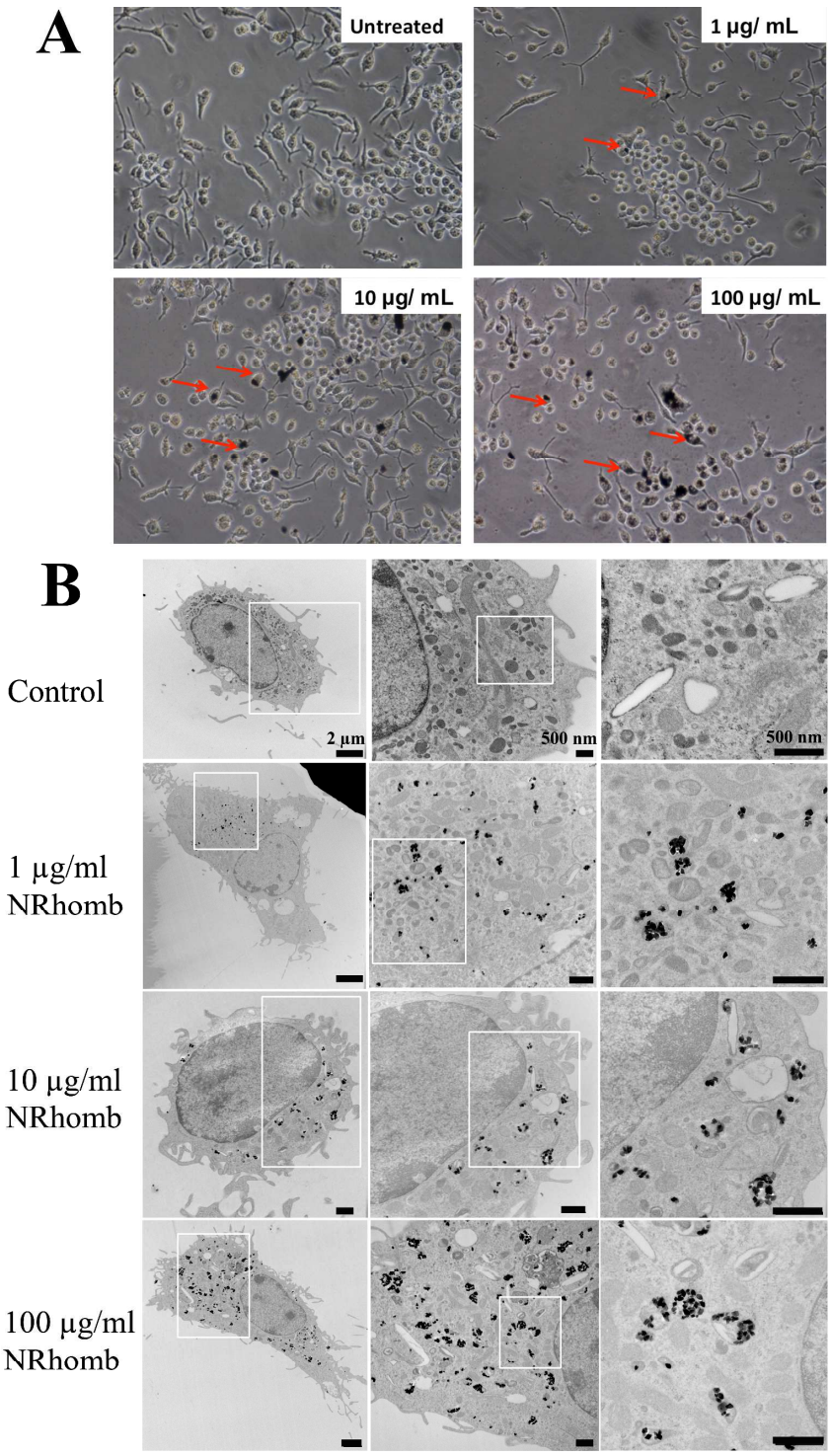

Figure 2. Cultured primary microglia engulf bare ~47 nm α-Fe_2O_3 N-Rhomb. Light microscopy images **(A)** of untreated cells and of cells exposed to 1, 10, and 100 µg/mL, respectively, of bare α-Fe_2O_3 N-Rhomb. Images were taken after 24 h after α-Fe_2O_3 N-Rhomb exposure. Red arrows point towards cells that have internalized α -Fe_2O_3 N-Rhomb. TEM images **(B)** of untreated cells and of cells exposed to 1, 10, and 100 µg/mL, respectively, of bare α-Fe_2O_3 N-Rhomb. High magnification images of control-treated microglia (RhB) and of 1 µg/mL α-Fe_2O_3 N-Rhomb (N-Rhomb)-treated microglia. Scale bars are either 2 µm or 500 nm.

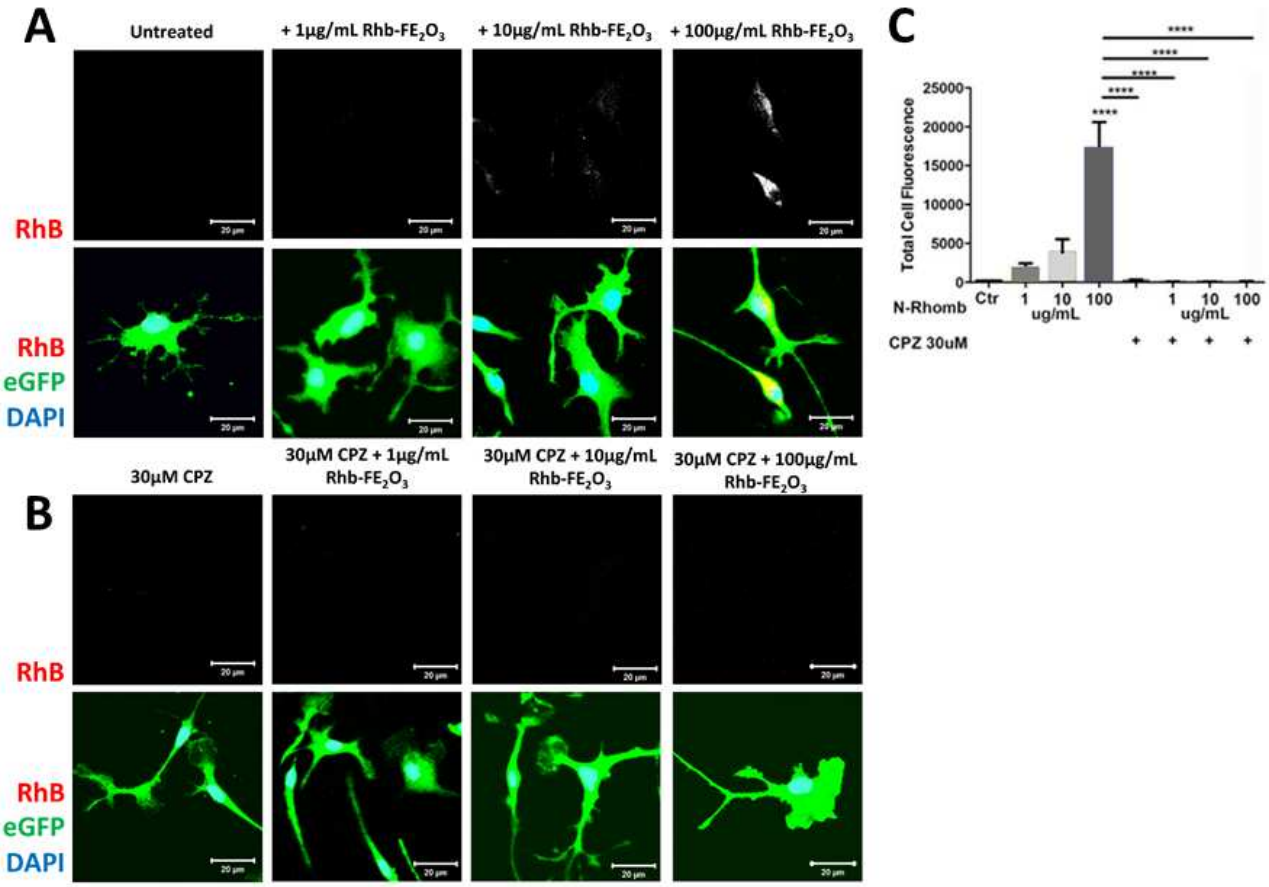

Figure 3. Primary microglia internalize RhB-labeled α-Fe_2O_3 N-Rhomb using a clathrin-dependent mechanism. (A). Confocal images of eGFP expressing microglia exposed to 1, 10, and 100 µg/mL, respectively, of RhB-labeled α-Fe_2O_3 N-Rhomb, stained with DAPI for nuclear staining. **(B).** Confocal images of cells exposed to 0, 1, 10, and 100 µg/mL, respectively, of RhB-labeled α-Fe_2O_3 N-Rhomb. Cells were pre-treated with 30 µM CPZ, 2 hours prior to nanoparticle exposure. Images were taken 24 hours after nanoparticle exposure. **(C).** Quantification of the RhB fluorescence of microglia treated either with or without 30 µM CPZ, followed by incubation with RhB-labeled Fe_2O_3 N-Rhomb. Scale bars = 20 µm. Data are shown as mean ± SEM. **** $p<0.0001$.

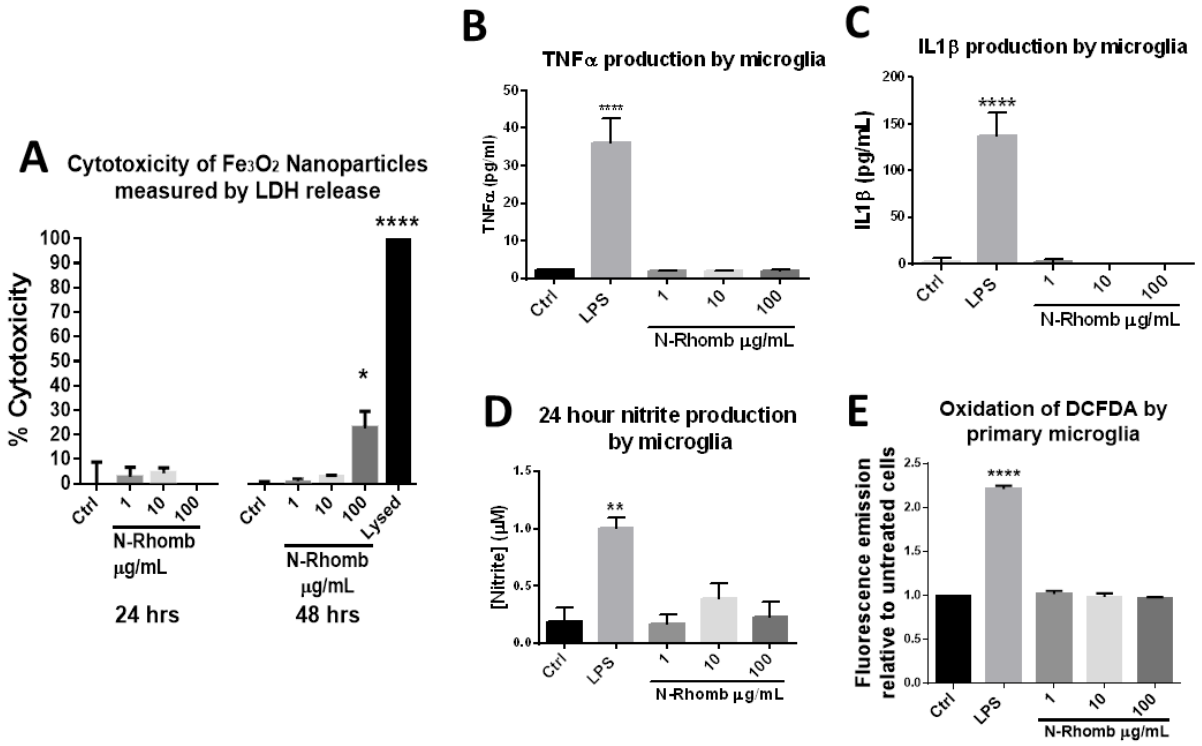

Figure 4. RhB-labeled α -Fe_2O_3 N-Rhomb are minimally cytotoxic and do not result in either the upregulation of pro-inflammatory factors or nitrite production within cultured microglia. (A). Conditioned media from primary microglia, treated with 1, 10, and 100 µg/mL, respectively, of α-Fe_2O_3 N-Rhomb were collected, and levels of LDH were measured at 24 and 48 hours. Untreated cells (Ctrl) served as a negative control and lysed cells served as a positive control for LDH release. **(B-C).** Primary microglia were treated with either 0 (Ctrl), 1, 10, or 100 µg/mL, respectively, of α-Fe_2O_3 N-Rhomb, or with 100 ng/mL LPS (LPS). Approximately 24 hours after treatment, media isolated from the cells were used for the detection of TNFα **(B).** or IL1β (**C**)**.** (**D**)**.** Nitrite production by primary microglia after 24 hours of incubation with 0 (Ctrl), 1, 10, or 100 µg/mL of α-Fe_2O_3 N-Rhomb, or with 100 ng/mL LPS. **(E).** Oxidation of DCFDA by microglia after a 24 hour incubation with 0 (Ctrl), 1, 10, or 100 µg/mL of α-Fe_2O_3 N-Rhomb, or with 100 ng/mL LPS. Data are shown as mean ± SEM. * $p<0.05$, ** $p<0.01$, **** $p<0.0001$.

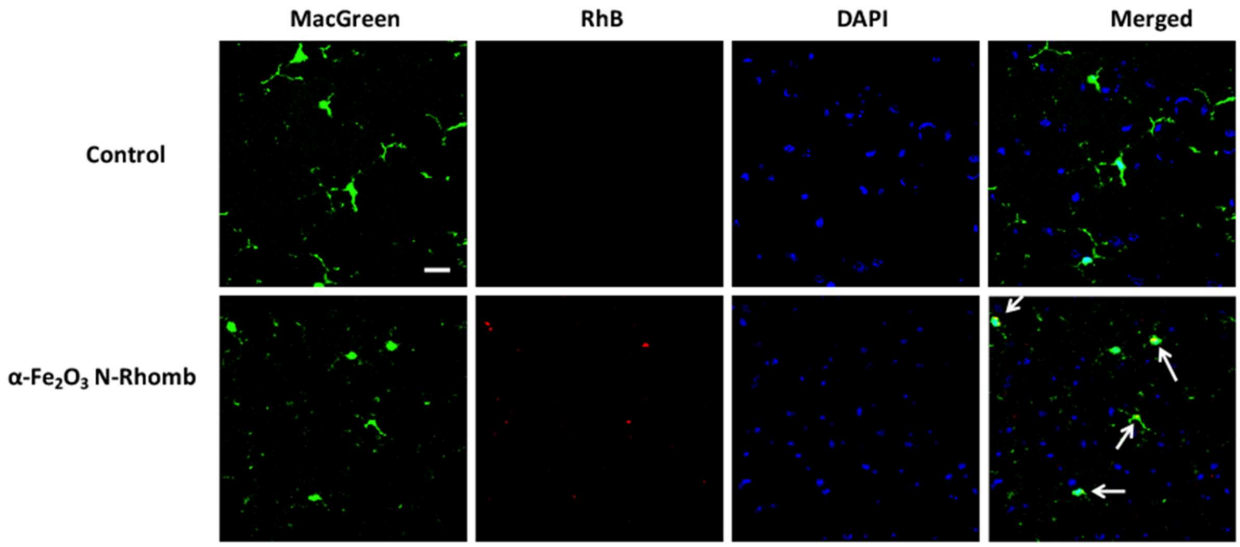

Figure 5. Microglia engulf RhB-labeled α -Fe_2O_3 N-Rhomb in vivo. Confocal images of brain sections from MacGreen mice treated with 100 μg/mL RhB-labeled α-Fe_2O_3 N-Rhomb. White arrows point towards microglia that have internalized the RhB-labeled α-Fe_2O_3 N-Rhomb. Scale = 20 μm.

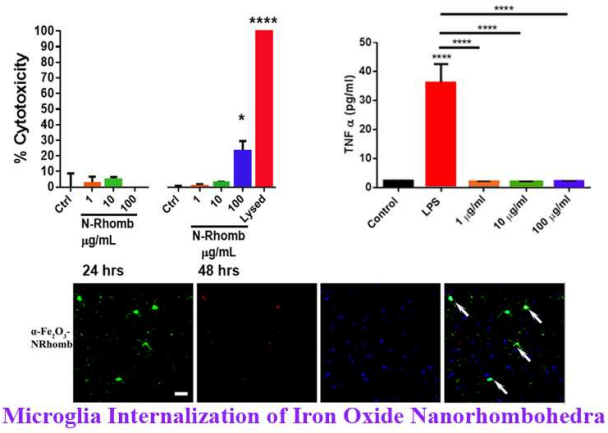

Microglia Internalization of Iron Oxide Nanorhombohedra

TOC Figure. We evaluated the cytotoxicity of iron oxide nanorhombohedra towards microglia cells, the first line of defense against disease in the central nervous system. The nanorhombohedra were modified with a fluorescent dye, Rhodamine B, in order to facilitate confocal imaging of their internalization within microglia cells. After 24 hours, we observed a less than ~4% cytotoxicity for all concentrations of incorporated nanorhombohedra. Moreover, upon nanoparticle internalization, we did not observe either any increased amounts of tumor necrosis factor alpha (TNFα) or nitrite production, thereby suggesting that these nanoparticles will neither promote dysregulation of TNFα responsible for various diseases nor stimulate the production of elevated levels of reactive oxygen species.